



Illinois State Water Survey

ATMOSPHERIC SCIENCES DIVISION

SWS Contract Report 503

DETERMINING THE CHEMICAL COMPOSITION OF CLOUD CONDENSATION NUCLEI

First Progress Report
Grant Number DE-FO2-90ER61017

by

Alien L. Williams, Jane E. Ruthert, and Kent E. McClure
Offices of Precipitation Quality and Atmospheric Chemistry
Illinois State Water Survey

and

Darryl J. Alofs, Donald E. Hagen, Daniel Ft. White, A.R. Hopkins, and Max B. Trueblood
Cloud and Aerosol Science Laboratory
University of Missouri, Rolla

Sponsored by:
United States Department of Energy
Office of Health and Environmental Research
Washington, DC

Champaign, Illinois
January 1991

ENR

Illinois Department of Energy and Natural Resources

**DETERMINING THE CHEMICAL COMPOSITION
OF CLOUD CONDENSATION NUCLEI**

**First Progress Report
Grant Number DE-FO2-90ER61017**

by

*Allen L. Williams, Jane E. Rothert, and Kent E. McClure
Offices of Precipitation Quality and Atmospheric Chemistry
Illinois State Water Survey
2204 Griffith Drive
Champaign, IL 61820-7495*

and

*Darryl J. Alofs, Donald E. Hagen, Daniel R. White, A.R. Hopkins, and Max B. Trueblood
Cloud and Aerosol Science Laboratory
University of Missouri, Rolla*

Sponsored by:
United States Department of Energy
Office of Health and Environmental Research
Washington, DC

Allen L. Williams
Principal Investigator

Champaign, Illinois
January 1991

Abstract.1
Introduction1
Continuous Flow Diffusion Chamber.7
Haze Chamber.8
Virtual Impactors.10
Ion Chromatography.12
Discussion13
References.18

Abstract

This report describes the design of a system to collect and chemically analyze cloud condensation nuclei (CCN). The basic approach is to identify which of the ambient aerosol particles are CCN by their ability to form droplets under supersaturated conditions, and to selectively remove the nucleated CCN from the background aerosol based on the inertial properties of the droplets formed. Design criteria and supporting discussion are advanced for the continuous flow diffusion chamber (CFD), the haze chamber, and the virtual impactors to be used in the experiments. Arguments are presented showing why the CCN sample must be divided into at least two parts for representative chemical analysis. Calculations are presented showing the behavior of a typical ambient aerosol as it passes through the collection system. The effect on the virtual impactor collection efficiency due to droplet growth inside the virtual impactor nozzle is considered. Results are reported from a collaborative chemical validation study for ion chromatography analysis.

Introduction

The only known method of determining the subset of atmospheric aerosol that act as CCN from a given ambient sample is to expose the sample to a supersaturated environment. The particles that form droplets at the cloud level supersaturations are CCN. Once activated the droplets will grow by diffusion in a supersaturated environment reaching, for example, 2.5 μm diameter in 1 second at 1% supersaturation. The CCN can be identified through their inherent ability to form droplets, and the droplets, once formed, quickly grow to large enough sizes that they can be removed from the ambient aerosol.

Important questions relating to the experimental design of CCN collection equipment involve the rate of CCN mass collection, and the ability to directly measure the composition of those CCN that are responsible for a large fraction of cloud droplets formed. An approximation of the size and mass distributions of the dry CCN particles can be made assuming that the spectrum, the number concentration of droplets, N , formed at critical supersaturation S_c , varies according to Twomey's relation¹ as

$$N = N_0 S_c^{1/2} \quad (1)$$

Assuming there are 1,000 particles nucleated at S_c of 1 percent, N_0 becomes 1000/cm³. The Kohler equations¹ yield the critical supersaturation of dry NaCl particles to vary as

$$D = 0.0232 S_c^{-2/3} \quad (2)$$

where D is the dry particle diameter in microns. Combining these

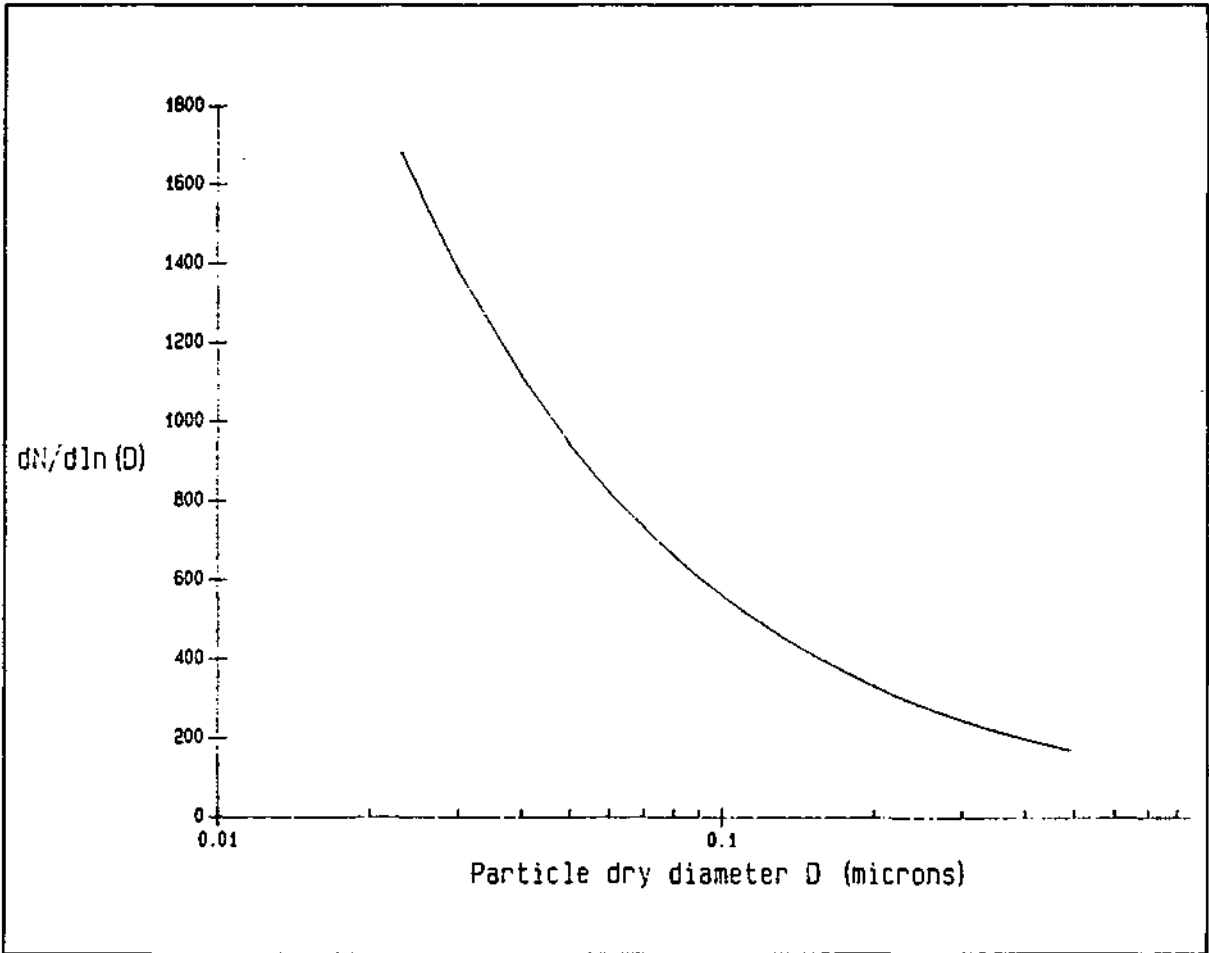


Figure 1. Number distribution of dry CCN particles derived from the droplet spectrum. The area under the curve is proportional to the CCN number concentration.

expressions gives N , the number of CCN with dry diameter greater than D ;

$$N = \frac{59.4}{D^{3/4}} \quad (3)$$

The resulting log-radius distribution is plotted in figure 1, and the corresponding log-mass distribution is plotted in figure 2.

In this example there are 941 particles/cm³ below 1 μm diameter, which represents a mass concentration of 20.75 pgm/m³. Seventy-one percent (70.7%) of these particles are below 0.1 μm diameter, and they account for only 0.112 μgm/m³ or 0.54% of the mass. In a cloud with a peak supersaturation of 1%, this example shows that most of the CCN would be from particles less than 0.1 μm diameter. The larger particles, representing over 99% of the mass, would completely determine the chemical composition of the CCN if they

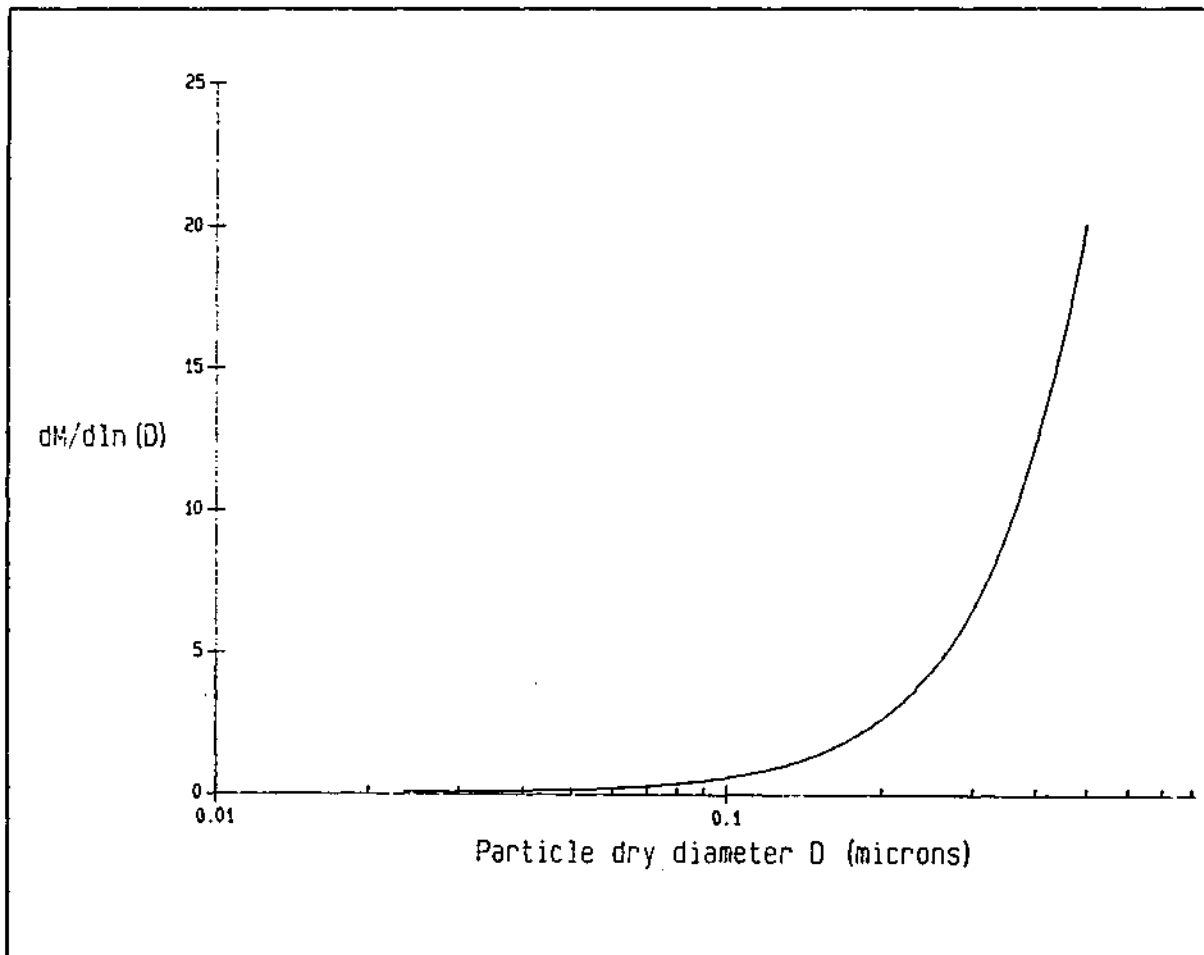


Figure 2 . Mass distribution of dry CCN particles derived from the droplet spectrum. The area under the curve is proportional to the CCN mass concentration.

were all collected together.

From the standpoint of the effects of CCN on cloud radiation, it is the number of cloud droplets formed that is of most significance. The nucleus in effect increases in size by a factor of hundreds as a cloud droplet is formed, and the CCN particles are changed from an invisible subset of the atmospheric aerosol to a dominant feature that reflects incident sunlight. Except for clouds with low peak supersaturations, it is the very small CCN particles that substantially determine the number of droplets formed. It is apparent that the small CCN must be collected and analyzed separately from the larger CCN particles. The sampling system being described here will separate the incoming sample into both a small CCN sample active at $0.16\% S_c$ 1% (dry NaCl diameter below $0.1 \mu m$), as well as a large CCN sample for nuclei active at $S_c < 0.16\%$ (dry NaCl diameter between $0.1 \mu m$ and $0.5 \mu m$).

If, as indicated in the above example, the small CCN are present in concentrations of order $0.1 \mu\text{g}/\text{m}^3$, it would be necessary to sample between 10 m^3 and 100 m^3 of air to obtain enough mass for chemical analysis. The flow rate contemplated is 1,332 lpm, so 10 m^3 of air could be sampled in 7.5 minutes, while 100 m^3 could be sampled in 1 hour and 15 minutes. The corresponding large CCN amounts collected during these sampling times would be $42 \mu\text{m}$ and $420 \mu\text{m}$ respectively. The prospect of collecting samples in such a short time is encouraging.

The CCN mass collection system consists of a series flow arrangement with a virtual impactor, followed by a haze chamber, another virtual impactor, a continuous flow diffusion chamber, and a final virtual impactor. Figure 3 shows a flow diagram of the system, and a schematic of the system is given in figure 4. Ambient air is first heated so that, upon leaving the haze chamber, it will be at the operating temperature of the CFD. The air then passes through the first virtual impactor, which operates at a cutoff size of $0.5 \mu\text{m}$. The fine particle flow of the first impactor passes into the haze chamber, where the particulate soluble material has time to absorb water and attain an equilibrium size. Aerosol particles exiting the haze chamber with sizes above 0.5 microns, which includes particles with dry diameter down to about $0.1 \mu\text{m}$, are collected in the coarse flow of a virtual impactor for analysis as the large particle CCN. The remaining aerosol is passed into the CFD operating at near 1% supersaturation. The activated droplets are grown in the CFD to form micron-sized cloud droplets that are removed by the third virtual impactor to become the small particle CCN sample. The final impactor is operated in a zero coarse flow condition to eliminate the mixing of inactivated fine aerosol with the small particle CCN sample.

The collection region of the final impactor will be flushed at a low flow rate by a carrier gas in order to deposit the CCN sample on a filter. In this way the sample can be placed on a filter for ease of handling. At low flow rates a small filter can be used to concentrate the sample into a small area, which is important for some analysis techniques. The low flow rates also allow the use of different filter types. A final advantage of flushing the sample region is to separate non-soluble nuclei. It is possible, thermodynamically, that wettable, non-soluble particles of diameter above $0.1 \mu\text{m}$ diameter can act as CCN, although diffusion battery experiments¹ as well as nucleation experiments² show the CCN to contain soluble material. In the collection system described, non-soluble CCN particles with diameter between $0.1 \mu\text{m}$ and $0.5 \mu\text{m}$ could be activated in the CFD and collected with the small CCN sample. In mixing with a dry carrier gas in the collection region, droplets would be evaporated leaving a bi-modal distribution with the non-soluble nuclei larger than the soluble nuclei. The larger particles could then be collected on a Nuclepore membrane allowing the smaller particles to pass for collection on another filter.

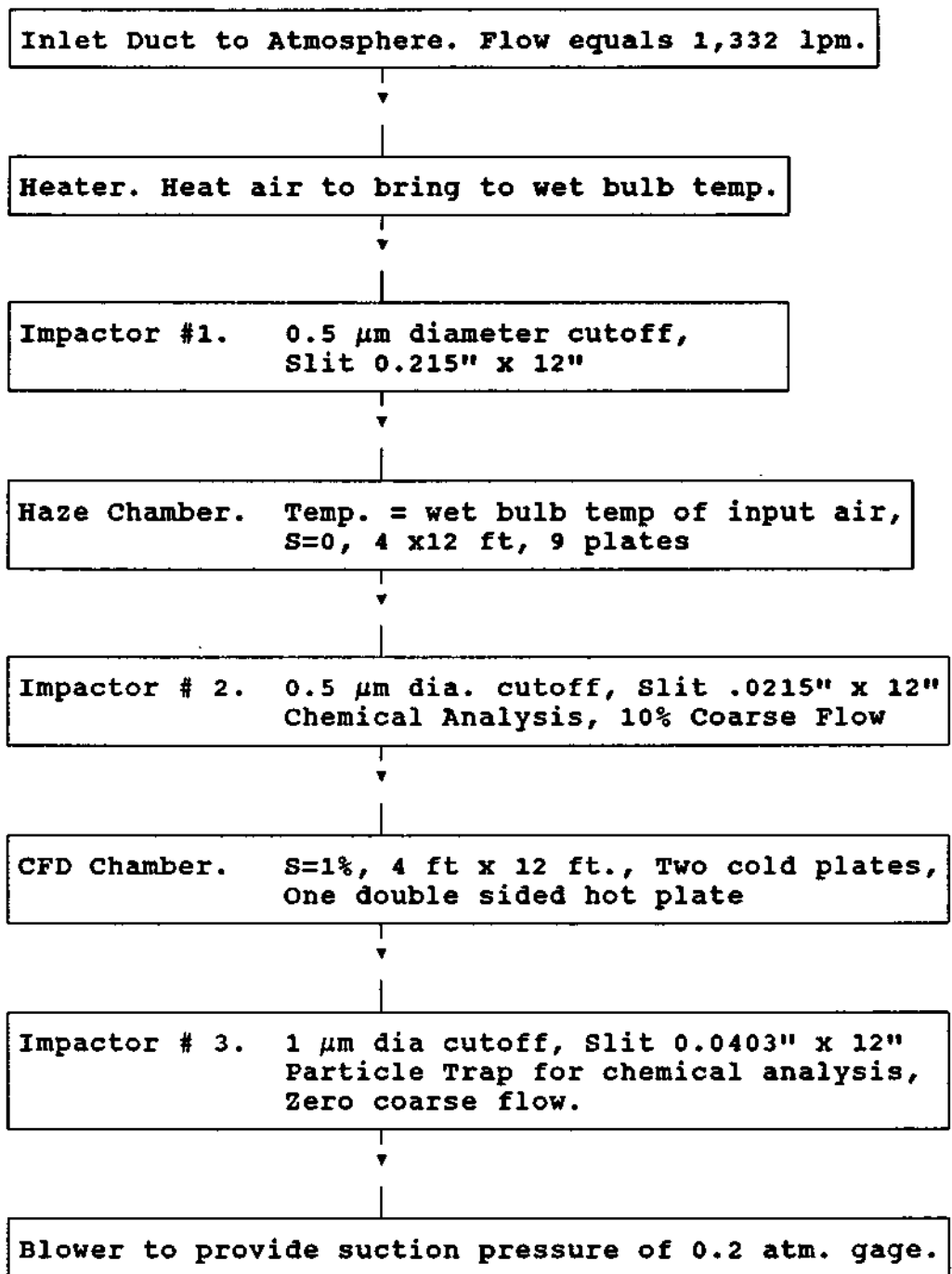


Figure 3. Components of CCN mass collection system

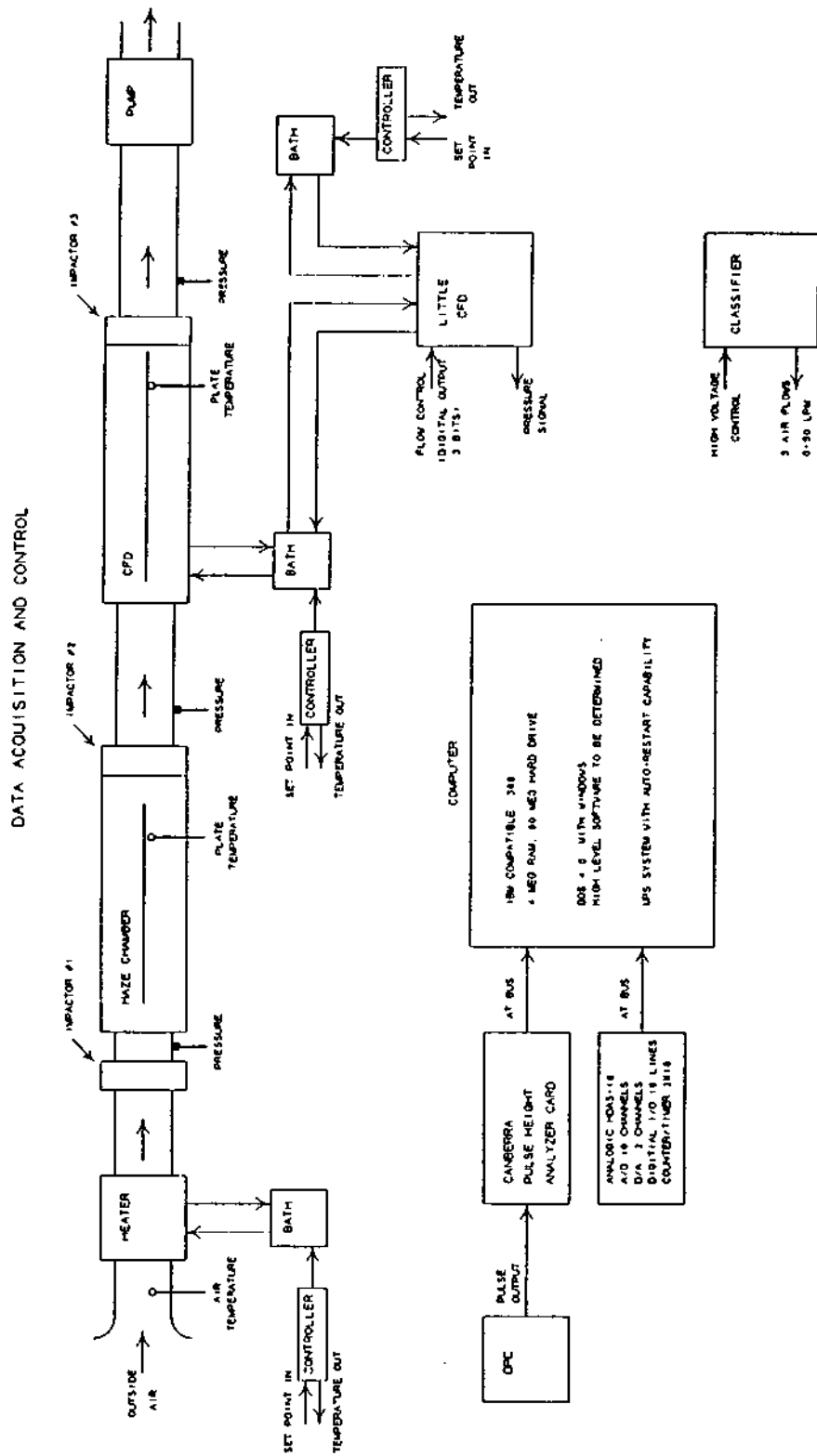


Figure 4. Schematic of CCN mass collection system.

Continuous Flow Diffusion Chamber

The volumetric flow of the entire system is essentially set by the flow capacity of the CFD. A rate of 1332 lpm is attained by building the CFD to stand 4 ft high and to flow horizontally along a 12 ft length. The design actually consists of two CFDs run in parallel. Figure 5 shows an expanded view of the CFD. The outer

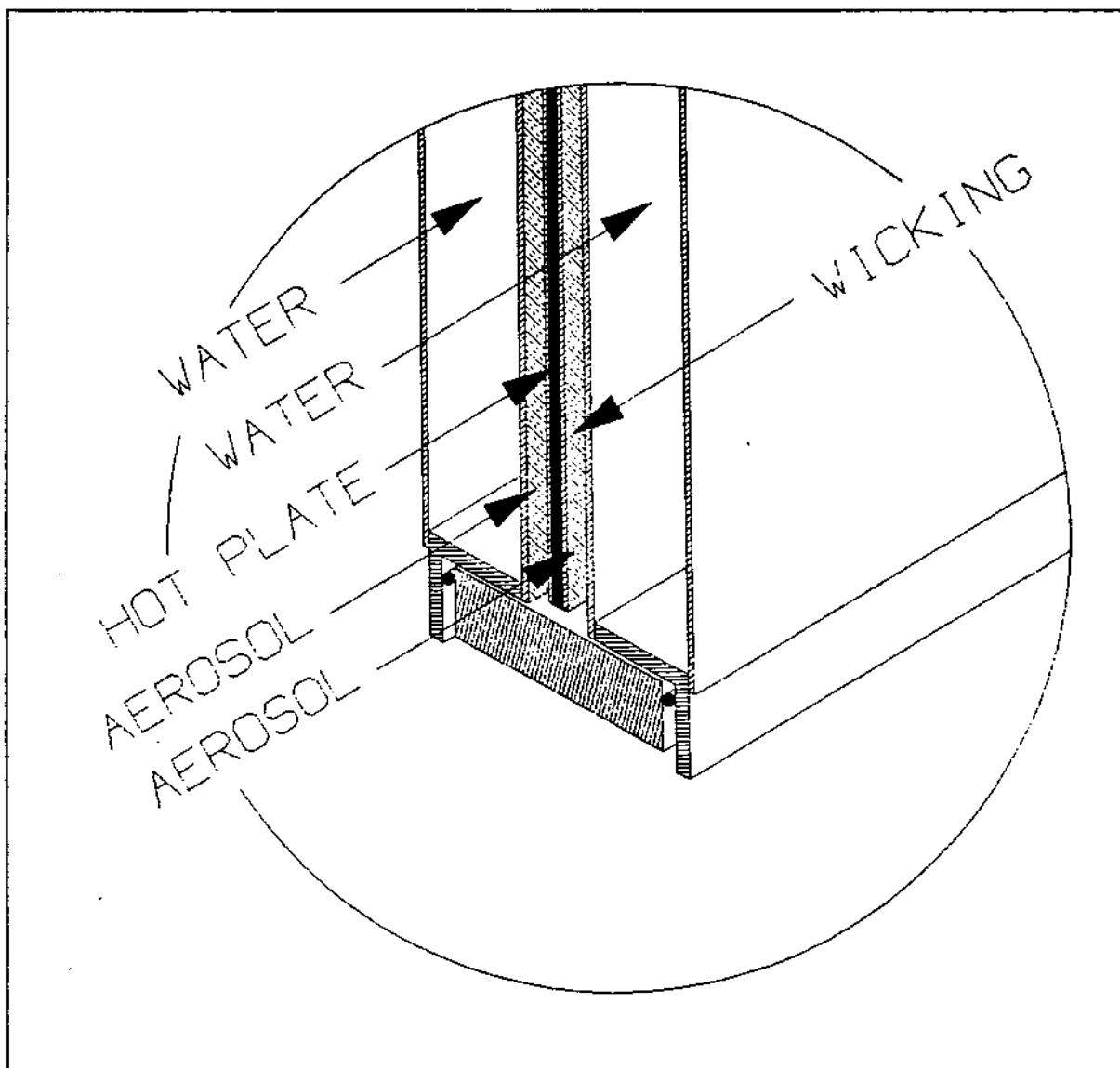


Figure 5. View of the CFD showing the water cooled outer plates, the common hot plate, and the supersaturated region.

walls are water cooled, and both are held at the same temperature by a single water bath. The inner common wall is electrically heated. The residence time of the sample in the CFD equals the time

necessary for the supersaturation to reach its equilibrium value, plus the time to nucleate and grow the droplets to super-micron sizes. The latter time is approximately one second for cloud conditions. Considering a parallel plate construction for the CFD, a plate separation of about 0.8 cm is optimum to maximize the volumetric flow per unit plate area. For smaller plate spacing the volumetric flow decreases, and for larger separations the time for the supersaturation to reach its final value becomes a large part of the total residence time in the chamber. The optimum total volumetric flow per unit plate area is about 150 lpm/m². Under these circumstances slightly over half the residence time is required for the supersaturation to equilibrate, so droplet nucleation and growth occur predominately in the latter half of the chamber.

The sample entering the CFD, after leaving the haze chamber and passing through the second virtual impactor, should contain only CCN with a critical supersaturation above about 0.16%. Due to the parabolic shape of the supersaturation profile of the CFD, near either wall where the supersaturation is below 0.16% no particles should be activated. Farther from the wall, where the supersaturation ranges upward from 0.16%, there will be CCN, with critical supersaturation below the operating value, that are not activated. This is, however, only a slight inefficiency of the CFD. No CCN outside the supersaturation range of from 0.16% to the maximum of say 1% would be activated, but due to the parabolic profile not all within that range will be activated. The fluid velocity profile across the CFD is also parabolic, so the CCN activated in the lower supersaturation region, and therefore subject to a slower growth rate, will experience compensatingly longer transit times, and exit the CFD at about the same diameter. It is unnecessary to introduce the plumbing complication of extracting only a part of the CFD flow for droplet collection.

Haze Chamber

Large CCN are separated from small CCN using a steady flow haze chamber with a virtual impactor at the exit. This function depends on the Laktionov³ relation

$$D_0 = \frac{.08}{S_c} \quad (4)$$

where D_0 is the equilibrium size of the nucleus at 100% relative humidity, and S_c is the nucleus critical supersaturation. Thus with a 0.5 μm diameter impactor cutoff, nuclei with S_c below 0.16% can be separated.

Since the virtual impactor proceeding the haze chamber removes all particles greater than 0.5 μm , the residence time in the haze

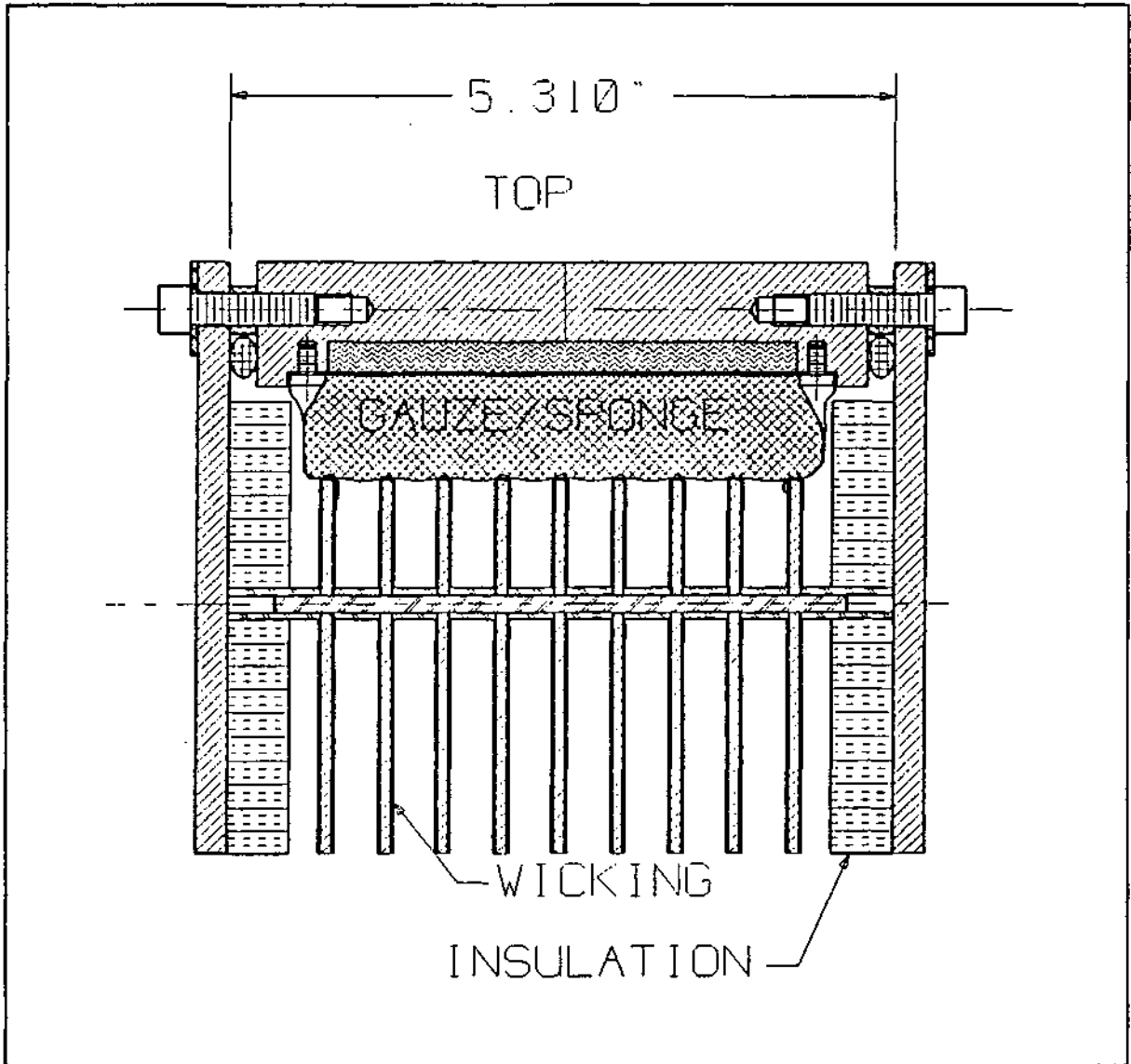


Figure 6. End view of the haze chamber showing the 9 wetted cloth racks inside an insulated box.

chamber must be sufficient for nuclei with $D_0 = 0.5 \mu\text{m}$ to grow to at least $0.5 \mu\text{m}$ diameter. To match the flow of the CFD, and allow time for the droplets to reach their equilibrium size, 860 square feet of wetted surface is required. The haze chamber will be 4 ft by 12 ft in dimension, and will consist of 9 parallel racks (plates) of wetted cloth in a parallel plate configuration with a 1 cm spacing. An end view of the haze chamber is shown in figure 6.

The haze chamber design has the simplicity of adiabatic cooling of the plates, thus avoiding the complication of active thermal control. Evaporative cooling of the plates by incoming sample air is compensated by the sensible heat transfer to the inlet air. As

a result, the plate temperature equals the wet bulb temperature of the incoming air. An analysis by Sparrow and Chen⁴ shows that the plates are very nearly isothermal. This is important in damping spurious supersaturations that could result if temperature gradients occur along the plates. During operation the inlet air to the haze chamber is merely heated to raise the wet bulb temperature of the sample air to the desired CFD inlet temperature.

Besides simplicity of construction, the haze chamber simplifies the flow management compared to an arrangement with 2 CFDs in series. Such a design would require extracting the central portion of the flow from the 1st CFD, which would be very complicated. To obtain the same volumetric flow as the present system, the first CFD would require twice the plate area as the CFD designed here.

Virtual Impactors

Virtual impactors with cutoff sizes of 0.5 μm , before and after the haze chamber, and a cutoff of 1 μm following the CFD are required. The operation of virtual impactors has received considerable attention (e.g., Marple and Chien⁵) and is well characterized. The cutoff efficiency varies as the square root of the dimensionless Stokes number, Sk , which can be written as

$$Sk = \frac{\rho V C D^2}{9 \mu W} \quad (5)$$

where ρ = the particle density, V = the nozzle velocity, C = the Cunningham slip factor, D = the particle diameter, μ = the fluid viscosity, and W = the nozzle diameter. The cutoff diameter can be found by solving equation 5 for D after setting $Sk=0.49$. By changing the nozzle diameter and flow velocity, the cutoff size can be adjusted over a considerable range.

The pressure drop through the impactor is an important parameter from the standpoint of the present application, since a single vacuum pump must draw the sample through all three impactors as well as the haze chamber and the CFD. The pressure drop across an impactor varies as V^2 , so designs that operate at small values of V are preferable. A 12 in. long slit design for the impactors has been chosen, with the slit width and other dimensions varied to obtain the two cutoff sizes required. A cross section of the device is shown in figure 7. The device is machined in two sections, and joined along the vertical broken symmetry line of the figure. Recommendations from work by Chen and Yeh⁶ are incorporated to lower the particle attachment to the impactor walls. A 12 in. slit with 0.108 cm spacing appears satisfactory for the 1 μm cutoff

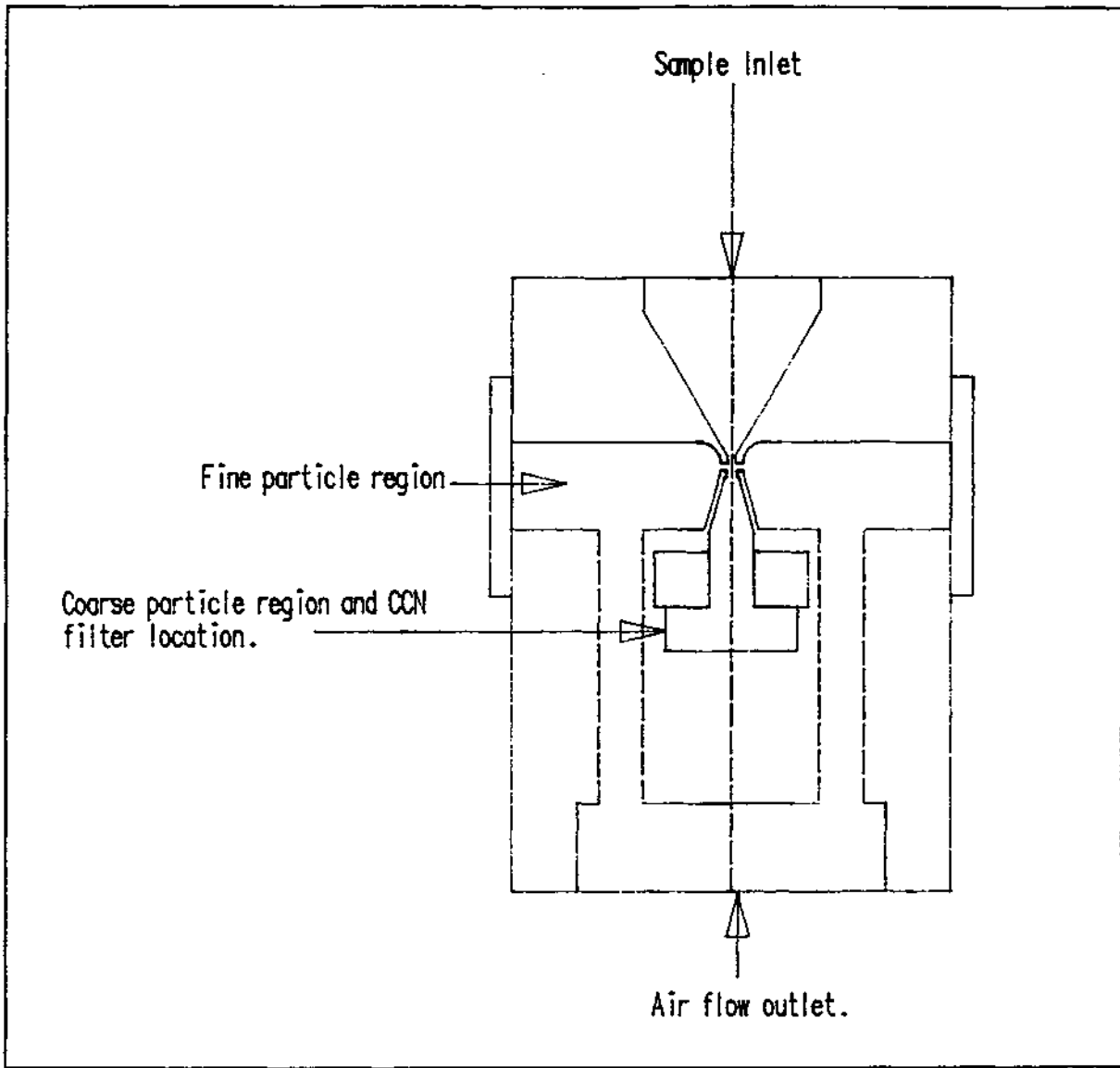


Figure 7. Cross section of virtual impactor design. Each of the two sections is 14 in. long, and they make a slit length of 12 in. when joined along the central broken line.

impactor, while the $0.5 \mu\text{m}$ impactors will consist of a 0.055 cm slit spacing.

The $0.5 \mu\text{m}$ cutoff impactors will operate with a filter in the coarse flow region, through which a small fraction of the total flow will be drawn. The filter from the impactor exiting the haze chamber represents the large CCN sample and will be kept for analysis. Sample air flow through the coarse flow region of the final impactor will be maintained at zero⁷ in order to reduce contamination in the small CCN sample. The droplets will be

inertially separated into the dead air space, just as with a conventional virtual impactor with a non-zero coarse flow. Tests are being conducted to determine if the sample volume can be flushed from the dead air space without altering the impactor cutoff efficiency, or causing background air and associated contaminants to be mixed in the sample air. The rate of flushing appears to be almost arbitrary, which could prove to be of significance for ease in handling the sample. As indicated, the sample could be filtered to selectively remove any large, non-soluble CCN. At low flow rates, the sample could be collected on very small areas, enhancing the utility of such analysis techniques as infrared microscopy.

Ion Chromatography

Several different chemical analysis techniques will be used for determining CCN composition. The possibility that trace amounts of different elements and compounds could indicate the origin of the CCN material, as is well known to be the case in ambient air samples, is an important aspect of the whole study. As it is commonly accepted that CCN are composed of sulfates, and particularly $(\text{NH}_4)_2\text{SO}_4$, ion chromatography stands out as an especially important technique. Comparison of the CCN composition with available data on the composition of material found in rain water and cloud water, which are often analyzed with ion chromatography, further emphasizes the importance of this technique. Results from an inter-laboratory validation study to test the accuracy of our equipment and techniques are given in Table I and discussed below.

Table I. Quality control sample summary.

Analytes	True Values (mg/l)	Average Lab Values (mg/l)	Average Differences (mg/l)	Acceptable Range (mg/l)
F	2.01	1.88	0.13	±0.2
Cl	10.00	10.34	0.37	±1.0
Br	5.00	4.96	0.17	±0.5
NO_3 (as N)	5.01	4.90	0.11	±0.5
HPO_4 (as P)	7.01	6.97	0.05	±0.7
SO_4	25.00	25.20	0.17	±2.5

The validation study effort was a part of the Joint USEPA/ASTM Collaborative Study for the validation of the United States Environmental Protection Agency (USEPA) Method 300.0, and the

equivalent American Society for Testing and Materials (ASTM) method. Seven anions (fluoride, chloride, nitrite, bromide, nitrate, monohydrogen phosphate, and sulfate) were measured using suppressed ion chromatography. The study was performed using three water matrices: reagent water (ASTM Type II), drinking or tap water, and a wastewater. This is the method that will be used for analyzing the cloud condensation nuclei (CCN), but the concentration levels are expected to be considerably lower than those in the collaborative study. The columns used in the ion chromatograph, when analyzing the wastewater and drinking water samples, were not those to be used for analyzing the CCN in order to avoid contamination of the columns. Final statistical results are not available from The Bionetics Corp., the company charged with conducting the study, but preliminary numbers are available. The true values of the test samples, although unknown during the test, are now available for comparison to the concentrations obtained during the study. The quality control samples furnished with the samples were analyzed three times. Table I shows the true concentrations, the concentrations obtained by this lab, the average differences between this laboratory and the true values, and the acceptable concentration range. Nitrite is not included in this table as there were problems determined in the study format that may render all of the nitrite data invalid. The other water matrices caused large interferences in the analysis, often resulting in the subtraction of two large numbers to obtain a small number close to the method detection limit, and are not reported.

Discussion

The capability of the haze chamber for separating the large and small CCN can be demonstrated for a particular case. Assume the aerosol entering the system has the shape of a Whitby distribution of soluble particles. From the Kohler equation the critical supersaturation for each dry particle size can be determined, and the resulting distribution is shown in curve 1 of figure 8. Here $\Delta N / \Delta \ln(S_c)$, the change in the number concentration, N , with respect to a change in logarithm of the critical supersaturation, S_c , is plotted versus $\ln(S_c)$, so the area under the curve represents the total particle concentration. For the flow rate of 1,332 lpm of the CCN collection system, the rate at which mass enters the system can be found for the assumed Whitby distribution, and is plotted in curve 1 of figure 9. This represents the number and mass that enters the first impactor. The particles that pass through the fine particle section of the first virtual impactor would be exposed to the 100% humidity environment of the haze chamber, and would reach their equilibrium sizes. The droplet concentration and particle mass flow rate that would be removed into the filter of the coarse flow region of the second virtual impactor are shown in curve 2 of figures 8 and 9 respectively. This corresponds to the large CCN sample. The droplets and particles separated into the fine flow, and therefore passing into the CFD, are shown in curve 3 of each figure. Since not all of the particles passing into the CFD would

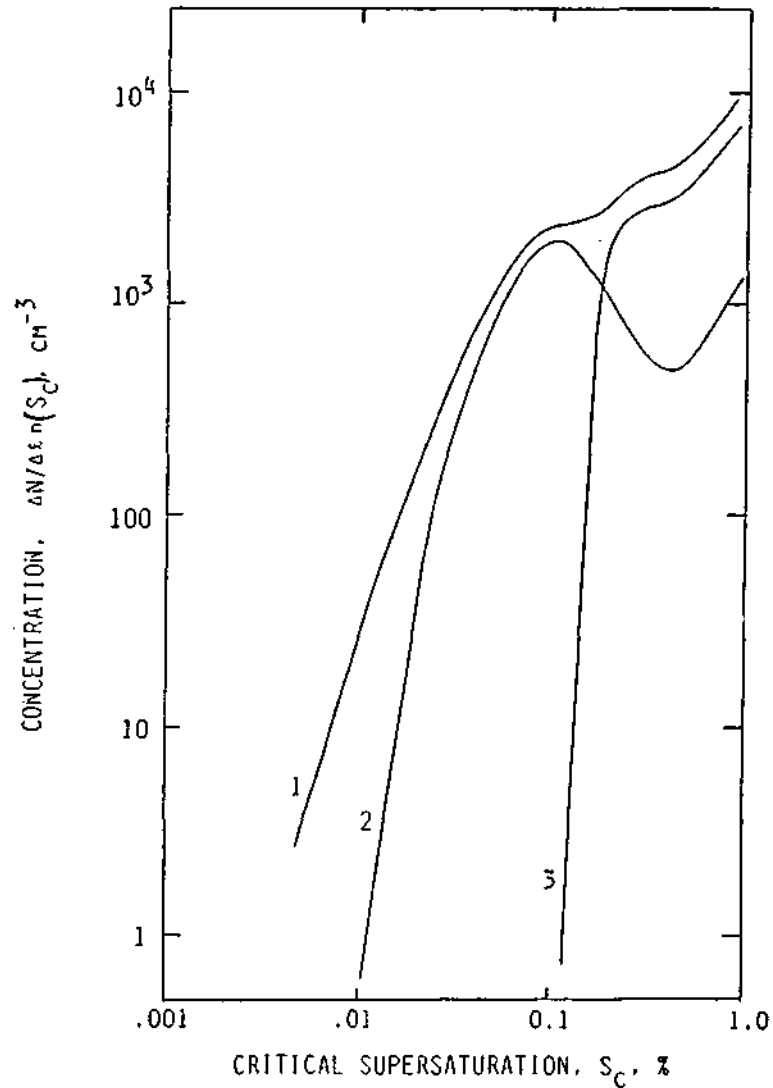


Figure 8. Log-supersaturation number distribution.
 Curve 1: Into first impactor, Curve 2: Into second impactor, Curve 3: Into CFD chamber.

be activated, curve 3 in each of the figures represents an upper limit to the small CCN sample. Comparison of the area under curves 2 and 3 of figure 8 shows that the small CCN represent larger numbers of particles than the large CCN. Similarly, the area under curves 2 and 3 of figure 9 shows that the large CCN account for

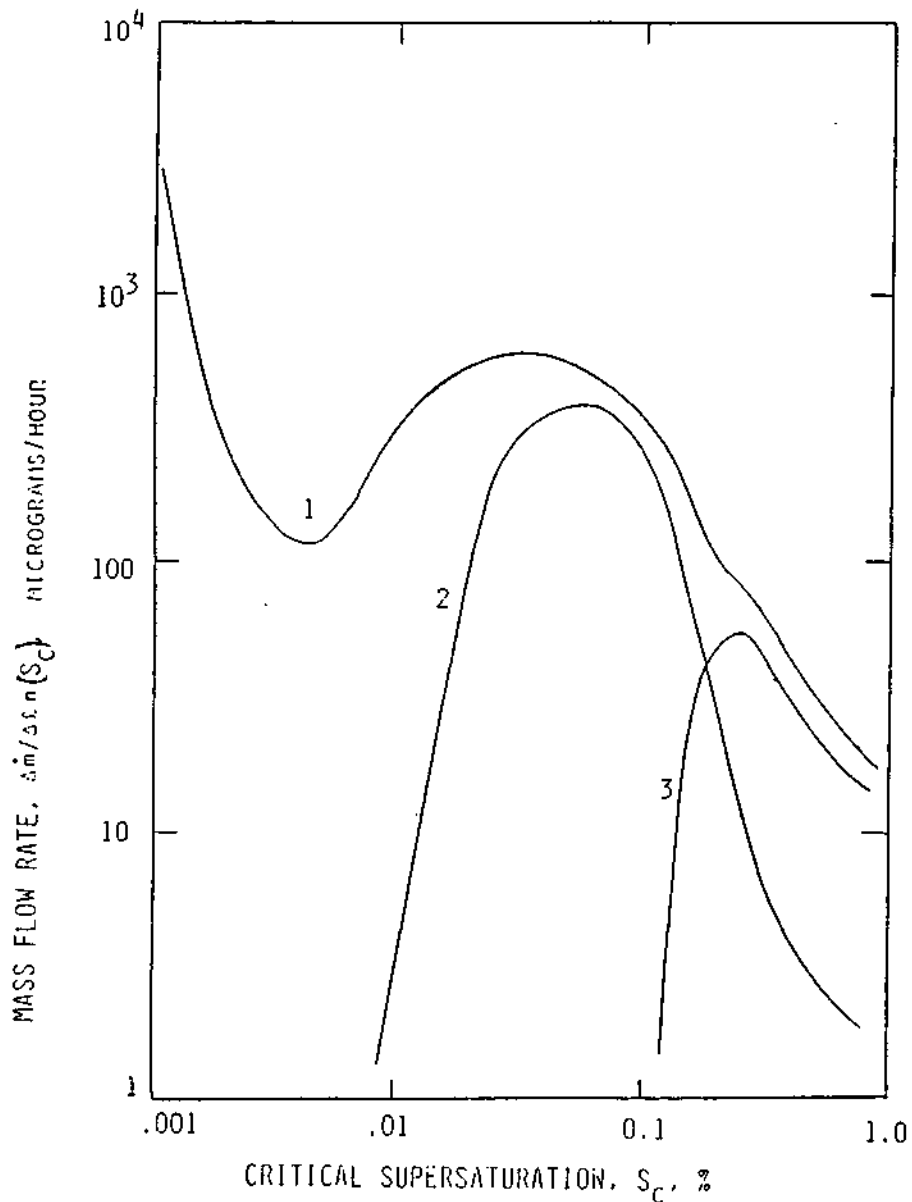


Figure 9. Log-supersaturation mass distribution.
 Curve 1: Into first impactor, Curve 2: Into second impactor, Curve 3: Into CFD chamber.

more of the mass. If the second impactor cutoff were 1.5 μm instead of 0.5 μm , so that CCN with dry diameter between 0.2 μm and 0.5 μm rather than between 0.1 μm and 0.5 μm were collected in the filter of the second impactor, the rate of mass collection of small CCN would be increased by a factor of 3.

The use of virtual impactors to separate droplets from the background aerosol raises the question of nucleation inside the virtual impactor. The pressure drop inside the nozzle of a virtual impactor behaves, in effect, like an expansion cloud chamber and produces a supersaturation. Using a potential flow model to estimate the pressure and velocity fields inside an impactor nozzle, and assuming an adiabatic expansion of already saturated air, the peak supersaturations turn out quite high, being in the range of from 70% to 300% over typical impactor flow rates. However, the time that a particle is exposed to the high supersaturations is only of order 10 μ sec. Particle or droplet growth could only increase sizes on the order of 10^{-3} μ m under these conditions, so in principle this is not a problem.

This question was also examined experimentally. NaCl particles were generated and passed through a classifier to remove all but a particular size. The particles were then passed into a haze chamber and allowed enough time to equilibrate. From the haze chamber the droplets were passed either through an impactor and then to a CFD, or directly to the CFD. An optical counter was used to determine the number of particles nucleated in the CFD. In this setup the CFD is essentially used as a detector to measure the CCN incident on the impactor, and the number passing through the impactor, from which the impactor efficiency can be determined. The experiment was then repeated for different dry particle sizes. Although the impactor was not a virtual impactor, but rather an inertial impactor with a nozzle diameter of 0.07 cm and a flow rate of 0.75 lpm, the efficiency should follow the same description. Figure 10 shows the experimental efficiency curve compared to the theoretical⁵ curve. The agreement is close enough to verify that the impactor is not nucleating and growing particles to sizes large enough to be inertially collected.

The CCN collection system is presently being built, and the prospects for success have improved. By increasing the sample flow over the original design, the constraints of long sampling times and small sample amounts appear to be eased. Introducing a more economical haze chamber into the system, rather than having 2 CFDs in series, has allowed the freedom of scaling up the system in size and volumetric flow while maintaining the same budget. Although a more realistic notion regarding the precise separation between large and small CCN will no doubt evolve as the actual sampling starts, the basic idea of the necessity of collecting at least two CCN size groups appears sound.

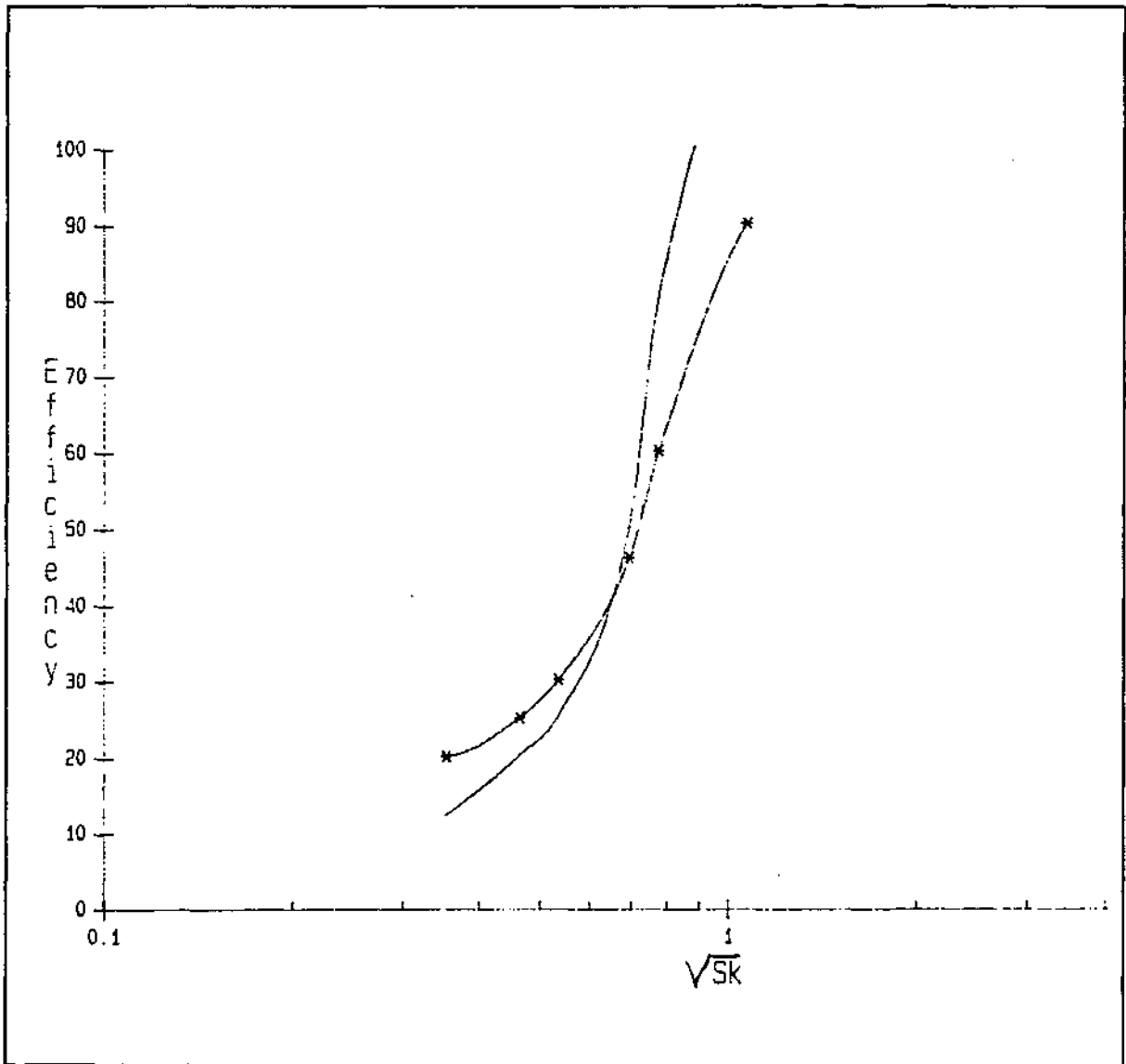


Figure 10. Experimental collection efficiencies compared to theoretical curve.

References

1. Twomey, S. A., 1977: Atmospheric Aerosols, Elsevier, New York.
2. Alofs, D. J., D. E. Hagen, and M. B. Trueblood, 1989: Measured Spectra of the Hygroscopic Fraction of Atmospheric Aerosol Particles, J. Applied Met., 28: 126-136.
3. Laktionov, A. G., 1972: A Constant Temperature Method of Determining the Concentrations of Cloud Condensation Nuclei, Izv. Acad. Sci. USSR, Atmos. Ocean Phys., 8, 382-385.
4. Sparrow, E.M. and T. S. Chen, 1969; Mutually Dependent Heat and Mass Transfer in a Laminar Duct, A.I.C.H.E.J., 15, 434-441.
5. Marple, V. A. and C. M. Chein, 1980: Virtual Impactors: A Theoretical Study, Environmental Science and Technology, 14, 976-984.
6. Chen B. T. and H. C. Yeh, 1987: An Improved Virtual Impactor: Design and Performance, J. Aerosol Science, 18, 203-214.
7. Biswas, P. and R. C. Flagan, 1988: The Particle Trap Impactor, J. Aerosol Science, 19, 113-121.